ChemPubSoc Europe

DOI: 10.1002/ejic.201800350

EurJIC European Journal of Inorganic Chemistry

Full Paper

Magneto–Structural Correlations

Magnetic Anisotropy, Magneto–Structural Correlations and Mechanism of Magnetic Relaxation in {$Dy^{III}N_8$} Complexes: A Theoretical Perspective

Tulika Gupta[a][‡] and Gopalan Rajaraman*[a]

Abstract: Ab initio CASSCF calculations have been undertaken to probe the origin of magnetic anisotropy in two structurally related {$Dy^{III}N_8$} SIMs {$[Dy(tmtaa)_2]^-$ and $[K(DME)_2][Dy(tmtaa)_2]$; **1** and **2**, respectively}. Our calculations reveal that complex **1** possesses a larger barrier for reorientation of magnetization (U_{cal}) than does **2**. This is essentially due to the intrusion of K^+ ions, which distort the geometry and the donor abilities of the ligands in complex **2**, compared with **1**. Moreover, the ligand field around Dy^{III} was found to stabilize $|m_J> = |\pm13/2>$ as the ground state, with stronger mixing by other $|m_J>$ levels. This corresponds to the observation of large g_{xx} and g_{yy} values at the ground state, leading to an efficient QTM process and very fast relaxation. The computed ground-state $|m_J>$ levels and the estimated g tensors for both complexes are in agreement with experimental results obtained from magnetic and EPR spectroscopic studies. In addition, we have developed various magneto–structural correlations for complexes **1** and **2**, in order to understand how small structural distortions are likely to influence the magnetic anisotropy. These correlations offer clues to enhancing the barrier height for magnetization reversal in {$Dy^{III}N_8$} complexes.

Introduction

Simplified analysis for the anisotropy of SMMs containing only one spin carrier, known as single-ion magnets (SIMs or mononuclear SMMs), has gained interest over the years, due to their superior SMM properties.[1] Magnetic anisotropy, owing to the unquenched orbital angular momentum of the lanthanide (Ln^{III}) inner 4f orbitals, and its inherent ability to interact weakly with ligands, is considered advantageous over transition-metal-ion-based SIMs.[2] One of the outstanding issues in lanthanide-based SIMs is to find a way to control the magnetic anisotropy[1d,3] and to quench the quantum tunnelling of the magnetization (QTM)[3a,4] effects. If these two goals are achieved, this will pave the way forward for high-density magnetic memories based on these molecules.[5,6] Lanthanide SIMs are also proposed for potential applications in the area of magnetic refrigeration,[7] molecular spintronics,[8] and quantum computing devices.[9] To harness the aforementioned technological benefits of SMMs, it is important to enhance the blocking temperature (T_B) beyond 300 K. To date, all reported SMMs are functional only at very low temperatures, with the exception of the $[Dy(Cp)_2]^+$ molecule, which exhibits blocking temperatures as high as 60 K.[6b,10] Although this is a significant breakthrough, enhancing the blocking temperature further is the need of the hour and several groups are actively working towards the synthesis of SMMs possessing larger T_B values.

Fine-tuning the local symmetry of the lanthanide ions, crystal-field strength, coordination number/geometry, and inter- and intramolecular exchanges have been considered as potential strategies for increasing the blocking temperatures of SIMs.[9,10c,10d,11] Additionally, a rigid ligand framework, without very low-lying vibrational states, is likely to help plug other leaks (by Raman/other mechanisms) in enhancing the blocking temperature.[12] To date, among all of the lanthanide-based SIMs, Dy^{III} (possessing an oblate-type 4f electron density for the ground $|m_J> = |\pm15/2>$ state) has indisputably conquered the credit of being the most prolific.[9b,9c,9e,10e,11b,11c,11h,11k,13] A strong axial ligand field stabilizes the $|m_J> = |\pm15/2>$ ground state for Dy^{III} complexes, facilitating favourable conditions to observe magnetic bistability.[3i,3j,14,15,25,16] Estimating the magnetic anisotropy and its directions are challenging, due to the complexity of ligand-field theory,[17] as well as a lack of symmetry in the ligand-field environment around the lanthanide ions. However, spectroscopic tools, such as inelastic neutron scattering,[18] multifrequency high-field EPR spectroscopy,[19] cantilever torque magnetometry[20] and single-crystal magnetometry,[21] have been successfully employed to probe the magnetic anisotropy. Despite the involved complexities, it is still challenging to extract detailed information about the direction of anisotropy from these experimental studies.

An alternative strategy to obtain insight into the magnetic anisotropy of lanthanide-based magnets is to employ state-of-the-art ab initio calculations, based on the wave function obtained from state-average complete active space self-consistent field (CASSCF)/superior methods. Recent developments in post-

[a] *Department of Chemistry, Indian Institute of Technology Bombay, Powai, Mumbai 400076, India*
E-mail: rajaraman@chem.iitb.ac.in
http://ether.chem.iitb.ac.in/~rajaraman/
[‡] Current address: Department of Chemistry, Institute of Science, Banaras Hindu University Campus, Varanasi 221005, India

Supporting information and ORCID(s) from the author(s) for this article are available on the WWW under https://doi.org/10.1002/ejic.201800350.

Hartree–Fock multiconfigurational ab initio methodology have been shown to be indispensable to envisage the magnetic anisotropy of SIMs and to endorse the magnetic anisotropy data procured from EPR spectroscopic measurements.[9b,9c,11i,13a,22] The CASSCF method, including spin-orbit interaction (RASSI-SO), has been found to reproduce the experimental data in several cases and its reliability towards calculating such intricate parameters is well established. In this regard, here, we have undertaken detailed ab initio CASSCF[23]/RASSI-SO[24]/SINGLE_ANISO[25] calculations, employing the MOLCAS[26] suite to study two recently[27] reported sandwich compounds [K(DME)-(18-crown-6)] [Dy(tmtaa)$_2$] (**1**) and [K(DME)$_2$][Dy(tmtaa)$_2$] (**2**) (H_2tmtaa = macrocyclic 6,8,15,17-tetramethyl dibenzotetraaza[14] annulene; DME = dimethoxyethane). Both of the complexes have been synthesized and characterized thoroughly using magnetic and EPR spectroscopic measurements. In both complexes, the central Dy^{III} ion is coordinated by two tetradentate $tmtaa^{2-}$ ligands and possesses D_{2d} (**1**) and C_{2v} (**2**) symmetry, respectively. Both compounds exhibit slow relaxation of magnetization in the presence of an external applied magnetic field of 100 Oe and the effective barriers (U_{eff}) are estimated to be 24.05 and 19.74 cm^{-1} for **1** and **2**, respectively.[27] While the core structure of the molecules are very similar, they possess different symmetry/structure with varying degrees of structural distortions. Here, by performing ab initio calculations, we intend to answer the following intriguing questions: (i) what is the origin of the non-Ising ground state observed in these complexes? (ii) what is the mechanism of the magnetic relaxation in **1** and **2** and how is their symmetry dictating these mechanisms? (iii) how do the structural parameters around the Dy^{III} ion influence the magnetic anisotropy, and hence, the energy barrier?

Computational Details

The MOLCAS 8.0[26] program package was utilized to perform post-Hartree–Fock ab initio calculations. To foster basis-set generation, scalar terms were included that were used successively to deduce spin-free wave functions and also energies, with the help of the complete active space self-consistent field (CASSCF)[23] method. However, spin-orbit coupling was incorporated using the RASSI-SO[24] method, which used the CASSCF wave functions as the basis sets and multiconfigurational wave functions as the input states. The resultant wave functions and energies of the pertaining multiplets were used for the determination of the anisotropic magnetic properties, crystal-field parameters and g tensors of the lowest state, using a specially designed routine SINGLE_ANISO.[25] Being inspired by our recent endeavour of basis-set appraisal in dictating magnetic properties of isotropic lanthanide systems,[28] we replicated that attempt in this study as well. We employed two basis-set approximations as adopted earlier:[13h] (i) Basis-set I (BS-I): [ANO-RCC...7s6p4d3f1g.] for Dy^{III}, [ANO-RCC...3s2p.] for C, [ANO-RCC...3s2p1d.] for N and O, [ANO-RCC...2s1p.] for H and [ANO-RCC•••5s4p1d.] for K; and (ii) Basis-set II (BS-II): [ANO-RCC...8s7p5d4f2g1h.] for Dy^{III}, [ANO-RCC...4s3p2d.] for N, O and C, [ANO-RCC...3s2p1d.] for H and [ANO-RCC...6s5p2d.] for K. The basis-set approximation for Dy^{III} was exactly adopted from the previous results.[13h] On the other hand, basis sets: ANO-RCC-VDZP for N, H, K and O atoms, ANO-RCC-VDZ for C atoms in the BS-I approximation, ANO-RCC-VTZ for N, C, K and O atoms and ANO-RCC-VTZP for H atoms in the BS-II approximation were adopted from the ANO-RCC library embedded in the MOLCAS suite.[29] The ground-state f-electron configuration for Dy^{III} is $4f^9$ and this yielded a $^6H_{15/2}$ multiplet as the ground state. First, we performed CASSCF calculations with an active space of nine active electrons in seven 4f orbitals (9,7). With this active space, we computed 21 sextets in the configuration interaction (CI) procedure.[11m] After computing these excited states, we utilized these computed SO states into the SINGLE_ANISO program to compute the g tensors. The Dy^{III} ion has eight low-lying Kramers doublets, for which individual states anisotropic g tensors were computed. The Cholesky decomposition for two electron integrals was employed throughout our calculations. Using the SINGLE_ANISO code, we also extracted the crystal-field parameters, as implemented in MOLCAS 8.0.[26] The transition matrix elements were computed using a MOLCAS routine provided by Prof. L. F. Chibotaru.[25] Subsequently, the magnetic properties of a single magnetic ion were calculated with a complete ab initio approach, where inclusion of spin-orbit coupling was being performed nonperturbatively. Structural optimization, Mulliken charges and the spin densities were computed using DFT calculations, by employing the Gaussian 09 suite.[30] Here, we employed the B3LYP[31] functional, along with the Cundari–Stevens[32] double-ζ polarization basis set, for the Dy^{III} ions, and the Ahlrichs triple-ζ basis set,[33] for the rest of the elements.

Results and Discussion

Our two concerned complexes (**1** and **2**) are comprised of the eight-coordinate Dy^{III} ion in a sandwich-type coordinating environment composed of eight N atoms from two $-tmtaa^{2-}$ ligands (see Figure 1a,b).[27] Complex **2** has an additional K^+ ion in proximity to the ring of four N atoms of one $tmtaa^{2-}$ ligand. The K^+ ion incorporation with one of the $tmtaa^{2-}$ ligands increases the pertaining Dy–N bond lengths by ca. 0.04 Å (i.e., 2.44 versus 2.48 Å for **1** versus **2**). Additionally, we have also measured the degree of distortion (S = 0 for a perfect polyhedron) in complexes **1** and **2**, as well as for the models employed in this study using eight-coordinate undistorted polyhedra (CU: cube; TT: triakis tetrahedron; TDD: triangular dodecahedron; SAPR: square antiprismatic; HBPY: hexagonal bipyramid; JSD: snub disphenoid). Both of the crystallographic structures of complexes **1** and **2** adopt geometries close to cubic, as the least deviations are found for this geometry (see Table S1 in the Supporting Information).

In **1**, the potassium (K^+) ion is coordinated by an 18-crown-6 ligand and one DME molecule has been detached from the $[Dy(tmtaa)_2]^-$core structure (see Figure 1a,b). Intrusion of the potassium ion into the $[Dy(tmtaa)_2]^-$ moiety provokes the reduction of the symmetry in **2**, compared with that in **1**.[27] To check the accuracy of our computed parameters, we have computed the magnetic susceptibility and magnetization data for both complexes utilizing CASSCF energies (see Figure S1). While

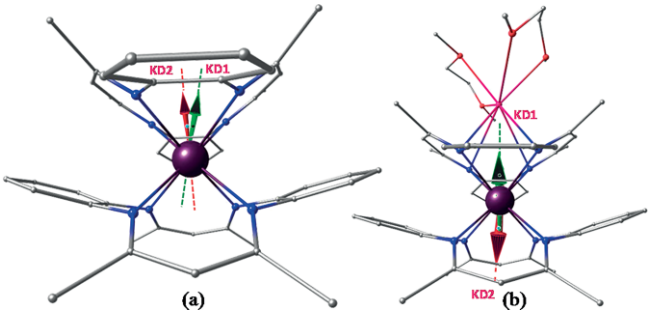

Figure 1. Ab initio computed g-tensor orientations along the *z* axis (g_{zz}) for the ground state (KD1) and the first excited (KD2) Kramers doublet for complexes: (a) **1** and (b) **2**. [Colour scheme Dy: purple; N: blue; O: red; C: grey; K: pink. All hydrogen atoms have been omitted for clarity].

calculations successfully reproduce the susceptibility data of both complexes, deviations are seen in the magnetization data. Computed ground-state anisotropies using the BS-I setup yield g_{xx} = 0.73, g_{yy} = 0.75 and g_{zz} = 16.85 for **1** and g_{xx} = 0.69, g_{yy} = 0.89 and g_{zz} = 16.82 for **2** (see Tables 1, S2 and S4). This infers an axial set of ground-state anisotropy associated with the large transverse components of the g-matrix (g_{xx}, g_{yy}). While experimental observations also reiterate a similar picture, the axiality of the computed g tensors is greater than that obtained from EPR spectroscopy (see Table 1). This deviation could be attributed to the absence of: (i) intermolecular/dipolar interaction in our calculated models; and (ii) metal-ligand covalency, which requires inclusion of ligand orbitals in the CAS reference space. Meticulous analysis of the g tensors reveals the occurrence of axiality, with significant g_{xx}, g_{yy} values, up to the fourth excited KD (KD5) and to KD7 for complexes **1** and **2**, respectively. Beyond the aforementioned levels, a drastic reduction of the g_{zz} tensor and a significant enhancement of the g_{xx}, g_{yy} values were detected (see Tables S2 and S4). In **1**, the g_{zz} axis of the ground-state Kramers doublet (KD1) passes along the principal C_2 axis through the centre of the upper –tmtaa^{2-} ligand (see Figure 1a) and deviates by ca. 48° and 57° from the right and left side of the N atoms, respectively.

Table 1. Ab initio computed principal values of the ground-state g tensors for the two studied complexes using two basis-set setups, along with the computed barrier height for magnetization reversal. Also, the CASSCF computed spin-free first (E_1) and second (E_2) excitation energies in cm^{-1} and the ($E_2 - E_1$)/E_1 parameters are given for complexes **1** and **2**.

	Complex **1**			Complex **2**		
	exp.	BS-I	BS-II	exp.	BS-I	BS-II
g_{xx} ($g^{\perp}$)	1.26[a]	0.73	0.78	1.41[a]	0.26	0.81
g_{yy}	–	0.75	0.81	–	0.57	1.02
g_{zz} ($g^{\parallel}$)	15.45	16.85	16.84	15.18	16.82	16.75
E_1	–	12.18	–	–	8.93	–
E_2	–	15.98	–	–	11.44	–
($E_2 - E_1$)/E_1	–	0.31	–	–	0.28	–
U_{eff}/U_{cal} [cm^{-1}]	24.05	87.67	79.37	19.74	76.27	68.98

[a] Experimental value obtained using X-band EPR spectra; only two g tensors, on diluted samples, are qualitatively derived.

A similar trend, observed in complex **2**, elicits the preferential alignment of anisotropy along the principal axis of symmetry, independent of electrostatic repulsion.[14b] The qualitative relaxation mechanism using the BS-I setup, for both complexes, clearly exhibits three possible ways for relaxation: (i) QTM within the ground-state doublet [i.e., |–13/2>↔|+13/2> (see Figure 2a,b)]; (ii) TA-QTM via excited states (i.e., |–15/2>↔|+15/2> in **1** and |–11/2>↔|+11/2> in **2**); and (iii) spin-phonon contribution to the relaxation (i.e., |–13/2>→|–15/2>→|+15/2>→|+13/2> in **1** and |–13/2>→|–11/2>→|+11/2>→|+13/2> in **2**). In both complexes, large g_{xx}, g_{yy} values in the ground KD are corroborated by pronounced QTM; that is, the corresponding

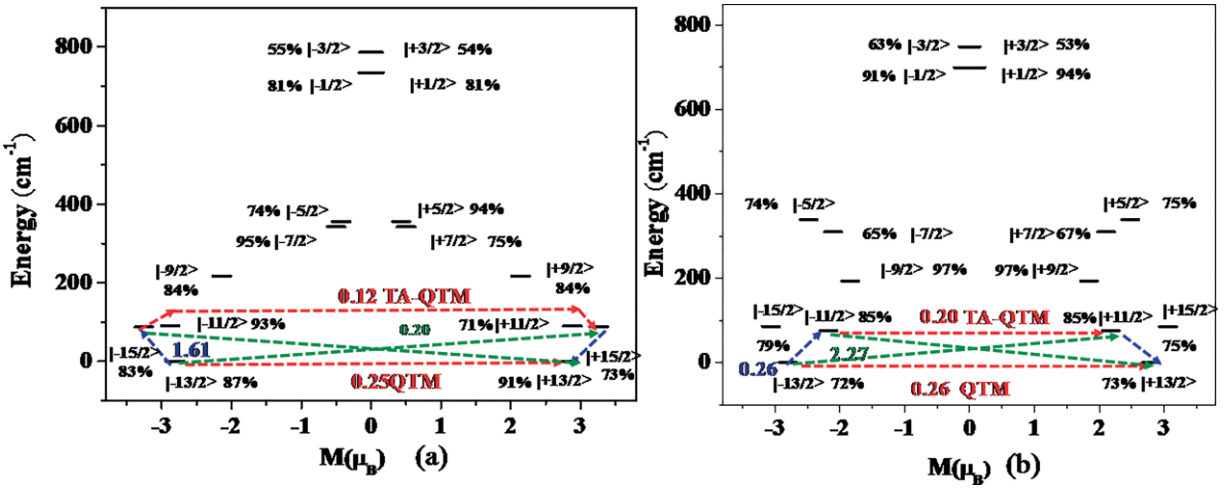

Figure 2. Ab initio computed electronic states, magnetic transition probabilities and magnetization blocking barriers for the ground $^6H_{15/2}$ multiplet of complexes: (a) **1** and (b) **2** in zero field. The *x* axis indicates the magnetic moment for each state along the main magnetic axis of the molecule. The thick black line indicates the Kramers doublets (KDs) as a function of the magnetic moment. The dotted green line indicates the plausible pathway of the spin-phonon process. The dotted blue line denotes the most probable relaxation pathways for magnetization reversal. The dotted red lines imply the presence of QTM/TA-QTM between the connecting pairs. All of the computed relaxation probabilities are dependent upon magnetic perturbation and are normalized from every departing state. For each Kramers doublet, the maximum contributing |±m$_J$> levels (percentage contribution) have been noted. Similarly, in all of the following figures of the relaxation mechanism, the corresponding depicted |±m$_J$> state possesses the maximum contribution to the particular wave function.

transversal-moment matrix elements are 0.25 and 0.26 μ_B for **1** and **2**, respectively (see Figure 2).The g_{zz}-KD2 (first excited KD) deviates by 9° and 170° for complexes **1** and **2**, respectively.

This non-concurrence with respect to the KD1-g_{zz} instigates relaxation via the KD2 state. This is nicely supported by pertinent transversal-magnetic-moment matrix elements, as 1.61 and 2.27 μ_B are obtained for **1** and **2**, respectively (see Figure 2). These two relaxation probabilities are in agreement with the experimental observations of the secondary process of relaxation, due to the presence of large transverse g-tensor components (see Table 1).[27] EPR spectra, recorded at 5 K, for these complexes reveal strong anisotropic signals. The observed $g_{||}$ endorses the $|m_J> = |\pm 13/2>$ ground state, with associated non-negligible g_{xx}, g_{yy} values, as evident from $g_{\perp} > 0$. An isolated pseudodoublet at the measured temperature and strong mixing of the wave function leads to the observation of features corresponding to the $|m_J> = |\pm 13/2>$ state, though the transition between these levels are formally forbidden.[34] However, the large QTM probability at the ground state reveals that both molecules are unlikely to exhibit SMM in the zero-field condition and application of a 100 Oe field is required in the experiments to clearly see the out-of-phase signals in the diluted samples of complexes **1** and **2**.

In the presence of an applied field, the QTM at the ground state is likely to be quenched to some extent, and this places the estimates of the calculated barrier height (U_{cal}) at 87.67 cm^{-1} and 76.27 cm^{-1} against the experimental U_{eff} values of 24.05 and 19.74 cm^{-1} for complexes **1** and **2**, respectively. Observed significant TA-QTM (corresponding matrix elements 0.12 and 0.20 for **1** and **2**, respectively) can be attributed to the large value of the associated transverse component of the magnetization in the first excited KD for both complexes. Disparity between the experimental and calculated values is anticipated, as the U_{cal} values given do not account for the large QTM probability observed at the ground-state level in both complexes. Moreover, intermolecular interactions and hyperfine coupling of the metal and the nitrogen atoms are likely to influence the barrier height and these are not factored into the estimates of the U_{cal} values.[22g] Additionally, fitting the ac data with an additional non-Orbach process is important to obtain a good numerical estimate of the experimental barrier height[22c,22f,35] and this has not been performed, also leaving some ambiguity as regards to the experimental estimates of the U_{eff} values. For **1**, the KD1 is predominantly $|\pm m_J> = |\pm 13/2>$: $0.87 \times |\pm 13/2> + 0.18 \times |\pm 11/2>$, while KD2 is preponderantly $|\pm m_J> = |\pm 15/2>$: $0.83 \times |\pm 15/2> + 0.60 \times |\pm 11/2>$. In **2**, KD1 is predominantly $|\pm m_J> = |\pm 13/2>$: $0.73 \times |\pm 13/2> + 0.19 \times |\pm 11/2> + 0.15 \times |\pm 5/2>$, while KD2 is prevalently $|\pm m_J> = |\pm 11/2>$: $0.85 \times |\pm 11/2> + 0.23 \times |\pm 9/2>$, astoundingly validating experimental results obtained from the EPR spectra (see Figure 2).[12b] Strong mixing of various $|\pm m_J>$ levels in the ground-state wave function is due to the presence of well-defined fourth-order transverse anisotropy, as expected in cubic symmetry. We have attempted to understand the role of the CASSCF computed spin-free energies in the magnetic anisotropy, as stated earlier.[36] Experimentally, the field-induced SMM behaviour of both studied complexes is reaffirmed by our computed small $(E_2 - E_1)/E_1$ parameter (see Table 1), which basically corresponds to lower axiality.

Analysis using the BS-II setup clearly reaffirms the axiality of the ground state, with huge transverse components of the magnetization for both complexes, as also seen in the BS-I setup (see Table 1, S3 and S5). The energy spectra for eight low-lying KDs arising from $^6H_{15/2}$ atomic term are found to span a range of 700 cm^{-1}, whereas subsequent excited states ($^6H_{13/2}$) are lying in a range of 3000 cm^{-1}. In this approach as well, the relaxation is found to occur via the first excited KD (U_{cal} is 79.37 and 68.98 cm^{-1} for **1** and **2**, respectively; see Figure S2). Detailed qualitative relaxation mechanism and wave function analysis for the BS-II setup resembles the BS-I observations. The only difference lies in the nature of KD2 for **1**, which is preponderantly $|\pm 11/2> = 0.91 \times |\pm 11/2> + 0.27 \times |\pm 9/2>$ ($|\pm m_J> = |15/2>$ for BS-I in **1**). Beyond the aforementioned multiplets, dramatic enhancement of the g_{xx}, g_{yy} values is noted in this approach for complex **2**. Another common factor in both setups is the mixed nature (percentage of the $|\pm m_J>$ contribution) of all of the KDs, due to the natures of their cubic/lower symmetry conditions.[2a,3i,11c,37] The $|\pm m_J> = |15/2>$ state of Dy^{III} has oblate electron density, and a strong axial ligand field preferentially stabilizes this state over the others. A conjugated double bond, associated with the $tmtaa^{2-}$ ligand, displaces the Dy^{III} ion out of the $-N_4$ plane, intruding structural distortions in both complexes.[27] This perturbation causes the dominant ground state to be $|\pm m_J> = |13/2>$, rather than the desired $|\pm m_J> = |15/2>$ state, in both complexes. Comparing the results obtained from the two basis-set assessments, we found diminution of ground-state–first-excited-state gap from 87.67 to 79.37 cm^{-1} and 76.27 to 68.98 cm^{-1} for **1** and **2**, respectively, upon moving from the BS-I to the BS-II setup (see Table 1). This conclusion articulates a reduction of splitting (U_{cal}) upon enhancement in the basis set and also a drop in the deviation between the computed and experimental values as we increase the basis set.[38] The slightly larger g_{zz} component of the g tensors for **1** than for **2** implies a larger magnetic anisotropy for the former than for the latter, and this is also in agreement with the experimental[27] results.[38]

The differences in the magnetic properties observed for **1** and **2** essentially originate from the divergence in the symmetry environment (pseudo D_{2d} versus C_{2v}) and the related structural distortions. Therefore, we decided to gain insights into the acquired spectrum of crystal-field levels by computing the crystal-field parameters depicting the splitting of the $^6H_{15/2}$ atomic multiplets. Crystal-field parameters are most suitable to understand the QTM effects subject to the negligible contribution of intermolecular and hyperfine interactions. The corresponding crystal-field Hamiltonian is given as:

$$\hat{H}_{CF} = \sum \sum_{k=-q}^{q} B_k^q \tilde{O}_k^q$$

where B_k^q and $\tilde{O}_K^q$ represent computed crystal-field parameters and the extended Stevens operator, respectively.[39]

From the computed parameters, (see Table S6) we can clearly see that, among three B_k^0 ($k = 2, 4, 6$) parameters, one is negative, while the other two are positive. Additionally, nonaxial B_k^q

($K \neq 0$, q = 2, 4, 6) parameters turn out to be larger than the axial B_k^q ($K = 0$, $q = 2,4,6$) terms. This implies a preferential equatorial ligand-field component, as compared with the preferred axial one. Moreover, additional intrusion by nonzero B_k^q ($K \neq 0$, $q = 2, 4, 6$) parameters play a proactive role in extensive mixing of the ground $|\pm m_J>$ wavefunctions and consequent nonzero $g_\perp$ components (see Table 1) due to a lack of rotational symmetry. However, notably, nonaxial B_k^q ($K \neq 0$; $q = 2, 4, 6$) are not imperative to induce pure, nonmaximal $|\pm m_J>$ ground states, as reported earlier.[40] This additionally substantiates the occurrence of a prevalent QTM contribution to the magnetization relaxation. The presence of large nonaxial terms, absence of crystallographic symmetry and asymmetric crystal-field interactions instigate ground-state QTM effect in both complexes. This consequently liquidates the SMM characteristics in both complexes. The application of the magnetic field causes the degeneracy of the $|\pm m_J>$ levels to be lifted, and the QTM effects to be suppressed, to a certain extent. This quenching of the QTM results in the observation of field-induced SMM behaviour, with two relaxation processes, as reported earlier.[41,42] A subtle difference in the axial B_k^0 parameters (**1** > **2**) induces larger magnetic anisotropy and barrier heights for complex **1** (see Table S6). Between these two complexes, the gradual disappearance of nonaxial B_k^q ($K \neq 0$; $q = 2, 4, 6$) terms with increasing symmetry is observed [for **2**, nonaxial B_k^q ($K \neq 0$; $q = 2, 4, 6$) terms are larger than in **1**; see Table S6].

We aim to further probe the electronic structure, the role of the crystal-field parameters, 4f ligand interactions and changes in the electrostatic potential. In this regard, we have undertaken detailed DFT calculations and analyzed 4f orbital energies, bonding, and spin densities. While DFT calculations are known to fail for strongly anisotropic systems, such as Dy^{III}, the bonding scenarios are expected to be qualitatively the same for various configurations, and hence, such analysis has been performed. The computed spin-density plots articulate a mixture of spin delocalization and polarization in complex **1**, with the observation of predominant spin polarization on the nitrogen donor atoms (see Figure 3c). For complex **2**, equal spin-delocalization and spin-polarization contributions have been observed (see Figure 3d). To ascertain the factors determining the differential behaviour in the complexes, we have performed molecular orbital (MO) analysis on both complexes. The magnetic anisotropy of the 4f electron density of the Dy^{III} ($4f^9$) centres are dictated by the nonspherical density distribution of the two β electrons.[36] In complexes **1** and **2**, the 4f–α orbitals are found to split with a large energy separation, suggesting a relatively stronger crystal-field effect on the 4f electrons (see Figure 3a,b). The splittings are apparently larger for **1** than for **2** for the 4f–α set. Importantly, calculations predict near-degenerate 4f–β orbitals in **1**, while splitting between the levels exists in **2** (see Figure 3a,b). This can be attributed to the intrusion of the K^+ ion inside the ligand cavity, altering the symmetry and the donor capability of one of the ligands. This larger splitting observed in **2** could be associated with the reduction of the orbital contribution, and hence, a lower barrier for magnetization reversal, as observed in the CASSCF calculations/experiments.

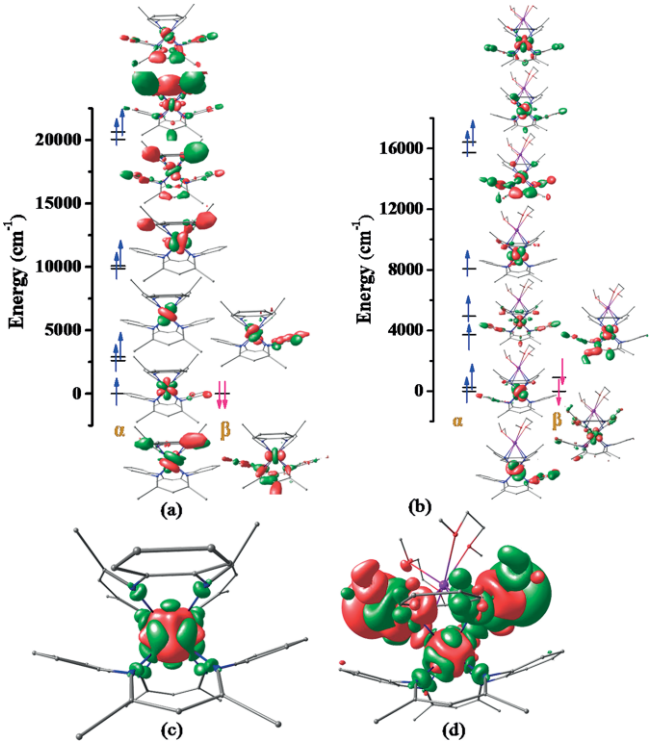

Figure 3. DFT computed α and β MOs representing the 4f orbitals with their corresponding eigenvalues for complexes: (a) **1** (left) and (b) **2**. DFT computed spin density plot for: (c) **1** and (d) **2**. The red and green regions indicate the positive and negative spin densities, respectively. The isodensity surface of the MO plot corresponds to a value of 0.01 $e^-/bohr^3$, while the spin density plots correspond to a value of 0.0003 $e^-/bohr^3$, since, in this instance, below this cut-off value, it is difficult to generate the contribution from the coordinating ligands.

How Do Structural Distortions Influence Magnetic Anisotropy?

Since the roles of the point-group symmetry, the electrostatic potential of the ligands, the effect of the ligand field and the coordination number in magnetization dynamics have been established by us and others,[9d,11c,11g,11i,22d,22g–22i,43] we are keen to understand the effect of the structural parameters on the magnetic properties. All of the following correlations have been performed employing the BS-I setup.

Magneto–Structural Correlations on Complex 1

To perform magneto–structural correlation in complex **1**, various possible distortions in the structure are surmised. This includes the Dy^{III} ion: (a) moving horizontally between the two sandwiched ligands (τ parameter, see Figure 4); and (b) moving vertically along the C_2 axis. Additionally, distortions of the ligands with variations in the Dy–N distances and other geometrical alterations are also attempted. These correlations are performed to understand how various structural distortions influence the magnetic anisotropy, although the distortions chosen are not the normal modes of vibration, as has been demonstrated elsewhere.[44]

Magneto–Structural Correlation for Parameter τ

In this correlation, the Dy^{III} ion is displaced horizontally from its original position, both in the left and right directions, compared

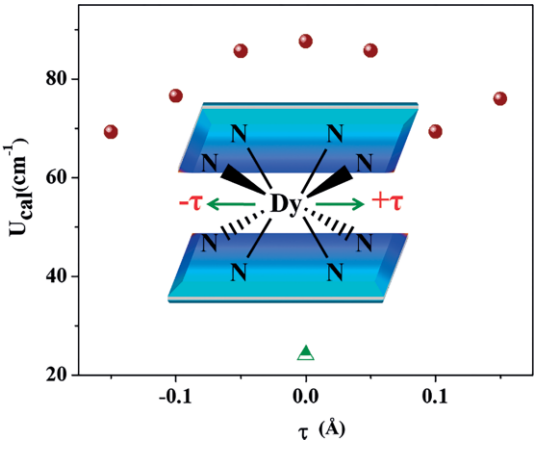

Figure 4. Performed magneto–structural correlation to observe the effect of the in-plane Dy^{III} horizontal displacement parameter (τ) on the U_{cal} value (the green triangle implies experimentally reported U_{eff} value for the X-ray diffraction structure).

with its original position in complex **1** (see Figure 4). The movement is denoted by the parameter τ, which describes the difference in the distance moved by the Dy^{III} ion, with reference to complex **1** (i.e., $\tau = 0$ denotes complex **1**). Here, the τ parameter is varied from –0.15 to +0.15 Å. As the ligand positions are unaltered, the Dy–N distances vary for these structures and this variation is found to be within ca. 0.2 Å. For all of the points computed, where $\tau \neq 0$, the ground-state anisotropy is found to be associated with large g_{xx}, g_{yy} components. This asserts the involvement of significant QTM towards the contribution of overall magnetization relaxation. In all of the models tested, g_{zz} is found to be ca. 17, with the stabilization of $|m_J> = |\pm 13/2>$ as the ground state (see Figure 5). This is also reaffirmed by our qualitative relaxation mechanism, developed on structures with selected τ values (see Figures 5 and S3 and Table S7). The first excited states of all models also possess substantial g_{xx}, g_{yy} values (see Figure 4 and Table S7). Additionally, the g_{zz} orientations of the first excited KDs (KD2, ϕ) are found to diverge significantly, with respect to the ground-state KD1, instigating relaxation via this state (benchmark angle of > 3°; see Table S7). This is reiterated by the significant matrix elements corresponding to the spin-phonon process (see Figure 5) for all our correlated structures. Due to dominant contributions from QTM and TA-QTM via the ground state and the first excited state, respectively, the U_{cal} value lies below 100 cm^{-1} in all of the structures studied. The developed correlation between the U_{cal} value and the τ parameter is shown in Figure 4; it reveals that the U_{cal} value gradually diminishes with both increases and decreases in the τ parameter. Computed g tensors, relative energies and ϕ angles are found to vary with variation in the τ parameter. This correlation reveals that all of the key parameters that control the magnetization reversal are only slightly perturbed by this distortion. Hence, this may not be the key structural distortion, which could drastically decrease/increase the barrier heights.

Magneto–Structural Correlation for Parameter α

Since the C_2 axis passes through the central Dy^{III} ion and amidst the two ligands, tuning the metal ion along the C_2 axis is likely to have greater perturbation on the magnetic anisotropy and the U_{cal} values. In this context, we have chosen to vary the parameter α. This is defined as the vertical displacement of the Dy^{III} ion in up/down directions with respect to the original X-ray diffraction structure, for which α is set to zero (see Figure 6 and Table S8). Moving the Dy^{III} ion up or down (notionally fixed) leads to positive or negative α values and for both of these points, an unsymmetrical ligand environment is expected. For example, for +α (–α) values, the Dy–N distance from the top (bottom) $tmtaa^{2-}$ ligand is expected to decrease (increase), while the Dy–N distance from the bottom (top) $tmtaa^{2-}$ ligand is expected to increase (decrease), creating an unsymmetrical ligand-field environment. Similar to τ correlation models, substantial g_{xx}, g_{yy} values have been observed in the KD1 and KD2 levels upon gradually varying the α parameter around the C_2 axis. For this correlation, a greater proportion of the g_{zz} variation is noted in the range of 12–16, and the relative energies of the ground to the first excited state are found to also vary

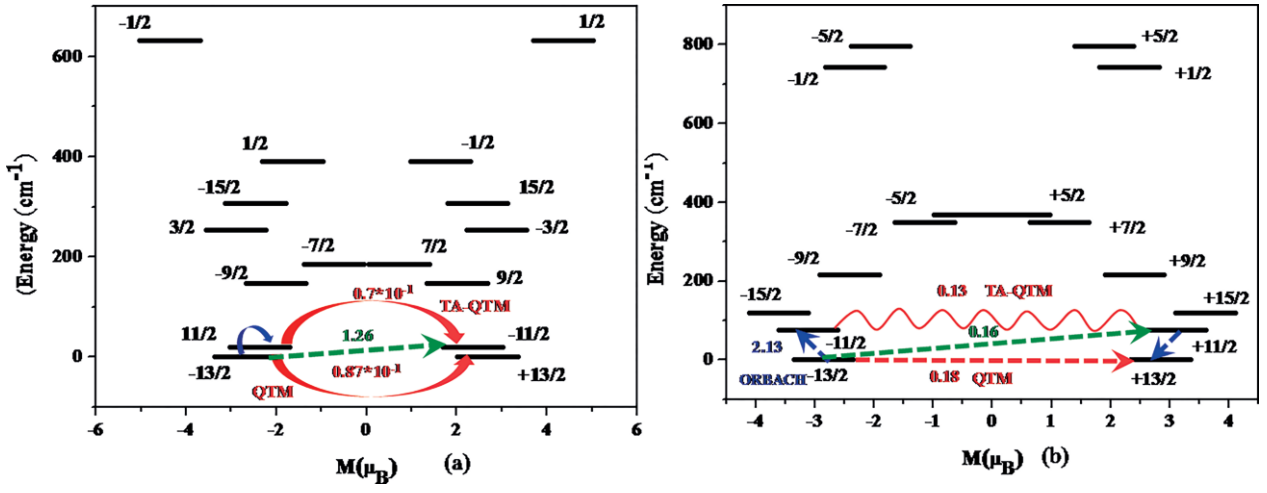

Figure 5. Ab initio computed electronic states, magnetic transition probabilities and magnetization blocking barriers for the ground $^6H_{15/2}$ multiplet of: (a) τ = –0.05 Å and (b) τ = +0.15 Å, created upon varying the τ parameter on complex **1** (for the X-ray diffraction structure of complex **1**, τ is taken as 0 Å).

grossly in the range of 15–128 cm^{-1}. The concomitant transverse component of the magnetization in KD1/KD2 in all models studied indicates the presence of prevalent QTM/TA-QTM. This is also nicely corroborated by our qualitative ab initio computed relaxation phenomena. Wave function analysis articulates KD1 as being predominantly $|m_J> = |\pm 13/2>$, asserting our observations on parent complex **1**. The KD2-g_{zz} orientation deviates (ϕ) largely with respect to the KD1-g_{zz} axis in all of the models studied (see Figure S4). This provokes relaxation via the KD2 multiplet, as confirmed by the large matrix element pertaining to the spin-phonon process (see Figure 6). With the aim of dissecting the variation in the g-tensor orientation upon changes in the structural parameters, we calculated the KD1-g_{zz} orientation for all models against the KD1-g_{zz} orientation in complex **1**. This divergence lies at ca. 0° to 120° (see Table S8). This suggests that this parameter is rather important in fine-tuning the anisotropy direction/barrier heights. If unsymmetrical ligands with variation in their donor capabilities are employed, this is likely to reproduce the trend observed with this parameter. With these, we attempted to develop a correlation between U_{cal} and the α parameter (see Figure 6). With both positive and negative α parameters, the estimated U_{cal} values are found to decrease monotonically. This is essentially due to the fact that as we move the Dy^{III} ion, the ligand interaction with the equatorial plane is enhanced and the axial interaction diminishes, leading to a drop in the estimated U_{cal} value (see Figure S5).

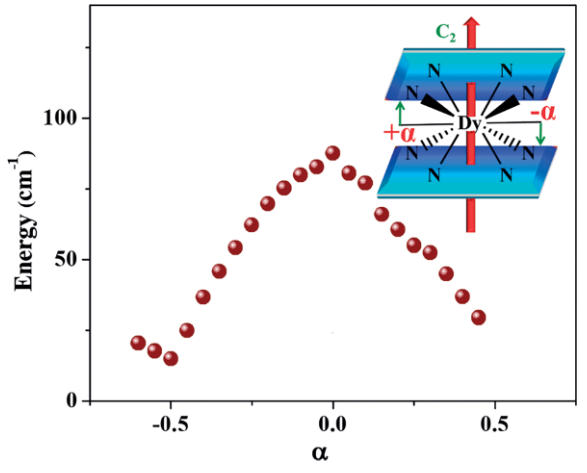

Figure 6. Developed magneto–structural correlation for probing the effect of the Dy^{III} ion, with respect to the variation of the α parameter and the computed U_{cal} values.

Magneto–Structural Correlation for Twist Angle Parameter (κ)

The eight nitrogen atoms of the ligand occupy the corners of the cube, leading to the core structure being close to the ideal CU structure. Here, we attempted to rotate one of the ligands, with an idea to generating square-antiprismatic geometry at 45° rotation. The X-ray diffraction structure of complex **1** is very close to the cubical structure, with a twist angle of only 2.5°. This twist angle parameter (κ) is varied from 0° to 25°. Calculations reveal a large variation (83–140 cm^{-1}) in the U_{cal} value as the κ parameter increases from zero. Moreover, as the κ value increases, the g_{zz} anisotropy is found to increase, leading to Ising behaviour (ca. 19.51) at higher κ values. Unlike our previous model studies, the g_{xx}, g_{yy} values do not prevail in this correlation. This paves the way for the observation that $g_{zz} \approx 20$, as expected for the pure $|\pm m_J> = |\pm 15/2>$ state in models possessing higher κ values (see Table S9 and Figure S6). This instigates the reduction of the QTM contribution for higher κ models. For models with a lower twist-angle κ, QTM remains prevalent. Since in all of the models, KD2-g_{zz} anisotropy deviates (ϕ) largely from the KD1-g_{zz} direction, relaxation preferentially occurs via KD2 (see Figure 7 for the significant matrix element corresponding to the spin-phonon process). The axial nature of KD1 is reduced, to some extent, in KD2, due to considerable contribution from the transverse g-tensor components (see Table S9). This correlates to considerable TA-QTM between the states of reverse magnetization pertinent to KD2 (see Figure 7). Models with a g_{zz} value of ca. 20 lead to the stabilization of $|\pm m_J> = |\pm 15/2>$ as the ground state, while deviation from $g_{zz} \approx 20$ results in the ground state being $|\pm m_J> = |\pm 13/2>$ (see Figure 8 and Table S9). While this correlation is found to

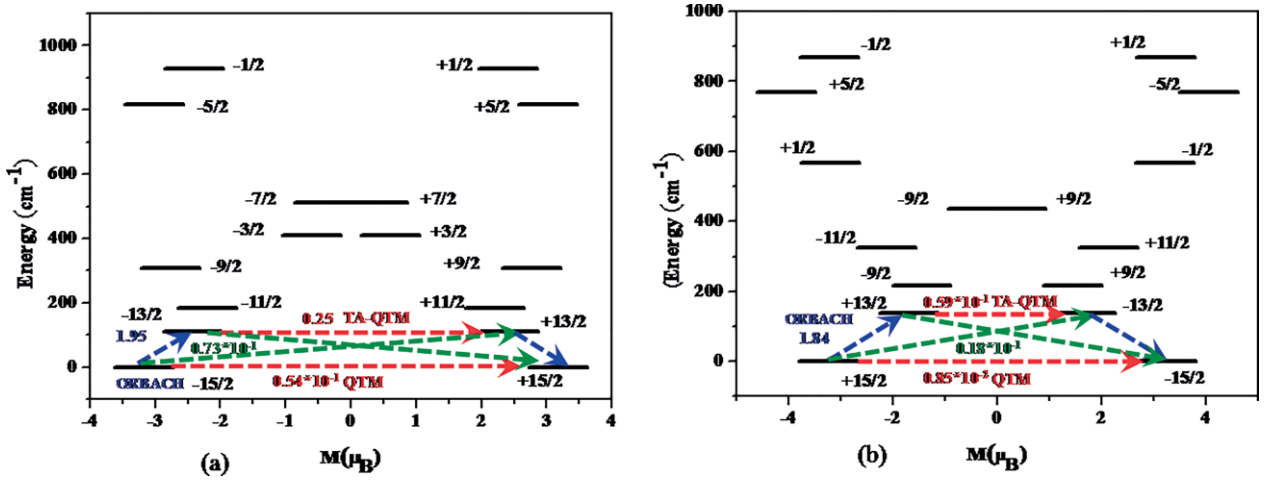

Figure 7. Ab initio computed electronic states, magnetic transition probabilities and magnetization blocking barriers for the ground $^6H_{15/2}$ multiplet of: (a) model with $\kappa = 4.6°$; and (b) model with $\kappa = 14.6°$ on complex **1**.

dramatically increase the barrier height and improve the g anisotropy, it is not surprising, in light of the performed experimental studies. It has been shown that an ideal square-antiprismatic geometry (with D_{4d} symmetry) best suits the Dy^{III} ion, and this leads to many SIMs possessing attractive blocking temperatures for this geometry.[3g,9f,35g,45,46] Our calculations suggest that a larger twist angle is likely to improve the magnetic properties of these systems and this could be achieved by appropriate ligand design.

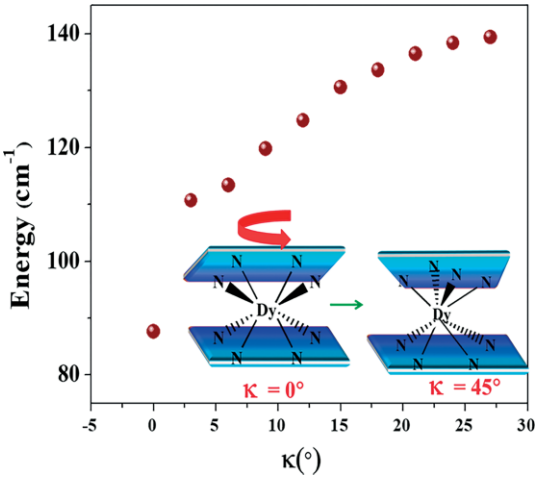

Figure 8. Magneto–structural correlation developed for the parameter κ.

Magneto–Structural Correlations on Dy^{III}···K^+ Distance

The main geometrical differences between complexes **1** and **2** are the presence of a K^+ ion near the ligand in complex **2**, while the same is found to be far away in **1**. Since the K^+ ion is close to the ligand environment, beyond the symmetry difference, the donor ability of the ligands to the Dy^{III} ion is also likely to be altered. To understand how this impinges upon the magnetic anisotropy, we have performed additional magneto–structural correlations pertinent to complex **2**. This correlation is performed by varying the Dy^{III}–K^+ distance. In complex **2**, this distance is estimated to be 3.83 Å, and this parameter is varied from 2.83 Å to 5.33 Å (see Table S10). The resultant correlation is shown in Figure 9. Models resulted from the variations in the K^+ ion position possesses significant g_{xx}, g_{yy} values in KD1 and KD2 multiplets (see Figure S9 for g_{zz} alignment). This is due to the appreciable QTM/TA-QTM process in all of the models (see Figure S10). Owing to the considerable ϕ values in all models, the corresponding spin-phonon process is prominent (see Figure S10 and Table S10), promoting relaxation via KD2. Deviation from the parent position in **2** could not produce larger U_{cal} values (see Figure 9), but ground-state g_{zz} alignment differs from the orientation observed in **2** (see Table S10).

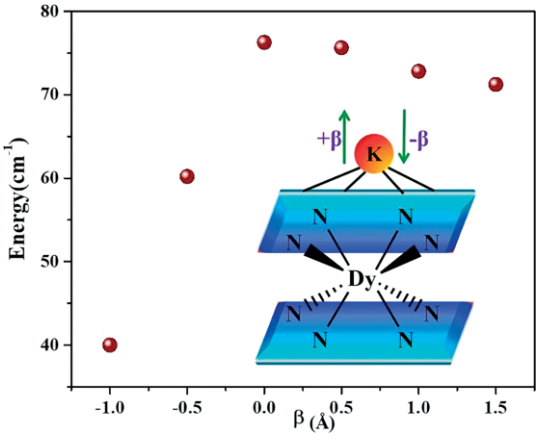

Figure 9. Magneto–structural correlation developed for parameter β on complex **2**.

Role of Substitution on Magnetic Anisotropy

Since the tetradentate $tmtaa^{2-}$ is ligated with the central Dy^{III} ion through four N donor atoms in **1**, the first coordinated sphere atoms are supposed to profoundly affect the magnetic anisotropy. Hence, we have decided to substitute the N donor atom in **1** with oxygen atoms (model **1a**) to gain deeper insights into the effect of substitution on magnetic phenomena (see Table S11). As lanthanide ligands are oxophilic, if such ligand architectures are made, stronger binding between the ligand and the Dy^{III} are expected, compared with complex **1**. In model **1a**, the KD1 (see Figure 10a for KD1-g_{zz} orientation)

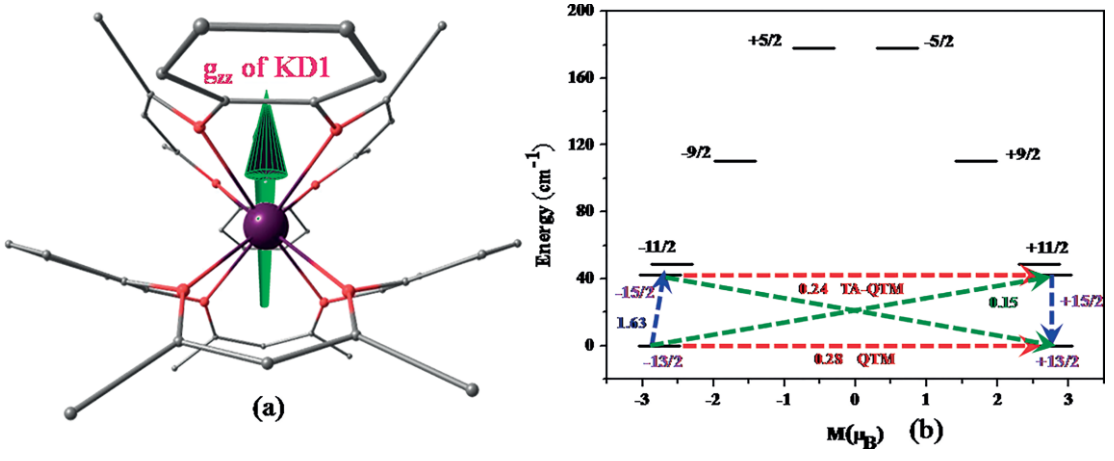

Figure 10. Ab initio computed: (a) ground-state g_{zz} tensor orientation for O substituted model; and (b) enlarged pictorial representation of electronic states, magnetic transition probabilities and magnetization blocking barriers for the ground $^6H_{15/2}$ multiplet of O-substituted model **1a**.

possesses huge g_{xx}, g_{yy} values (g_{xx} = 0.85, g_{yy} = 0.86, g_{zz} = 16.57). This is reiterated by appreciable QTM (pertinent matrix elements as 0.28 μ_B for **1a**) in our qualitative relaxation phenomena (see Figure 10b). Despite the smaller ϕ value of the excited multiplets in **1a**, huge concomitant g_{xx}, g_{yy} values ($g_{xy} > 0.5$) have spurred relaxation via KD2, as supported by QTM/TA-QTM (corresponding matrix element 0.28 and 0.24 μ_B, respectively; see Figure 10b). Thus, the overall pathway outlines U_{cal} as being 42.25 $cm^{-1}$for model **1a**.

Conclusion

Owing to the large magnetic moment, Dy^{III} based magnets are the most widely studied SIMs to date. Here, we have performed detailed ab initio post-Hartree–Fock calculations on two experimentally reported field-induced SIMs, where ground-state $|\pm m_J>$ levels and the corresponding g-anisotropies are unequivocally established using EPR spectroscopy.

Both complexes **1** and **2** lack pure Ising g tensors in their ground state, owing to the nature of the ligand field present. The presence of large g_{xx}, g_{yy} values leads to significant QTM/TA-QTM (via the first excited state) processes, rationalizing the field-induced SIM behaviour noted for both complexes. The decrease in the energy barrier for complex **2**, compared with **1**, is attributed to the reduction of the symmetry and the weakening of the Dy–N interactions in **2**, due to the presence of a K^+ ion in proximity to one of the ligands. Both the estimated g anisotropies and the ground-state $|\pm m_J>$ values are in agreement with the experimental results obtained from EPR spectroscopy, offering confidence in the computed parameters. For the first time, several magneto–structural correlations, corresponding to the possible structural distortions, have been performed to analyze and understand how such distortions influence the magnetic anisotropy and the barrier heights for magnetization reversal. In particular, the horizontal movement of the Dy^{III} ion (τ parameter) is found to only marginally influence the associated spin Hamiltonian parameter. However, other parameters, such as the vertical movement along the C_2 axis (α parameter) and the twist-angle corresponding to the conversion of a cubic structure to a square antiprism (κ parameter), are found to have profound impact on the estimated g tensors, its orientations and estimated barrier heights. These results broadly support the general observation of improvised magnetic properties for Dy^{III} complexes possessing square-antiprismatic geometry.

Acknowledgments

G. R. would like to thank SERB (EMR/2014/000247) for financial support. T. G. is grateful for a University Grants Commission (UGC) fellowship.

Keywords: Dysprosium · Magnetic properties · Sandwich complexes · Computational chemistry · Magneto–structural correlation

[1] a) N. Ishikawa, *Polyhedron* **2007**, *26*, 2147–2153; b) J. Dreiser, *J. Phys. Condens. Matter* **2015**, *27*, 183203; c) S.-D. Jiang, B.-W. Wang, S. Gao in *Advances in Lanthanide Single-Ion Magnets*, Springer Berlin Heidelberg, **2014**, pp. 1–31; d) Y.-S. Meng, S.-D. Jiang, B.-W. Wang, S. Gao, *Acc. Chem. Res.* **2016**, *49*, 2381–2389.

[2] a) J. Luzon, R. Sessoli, *Dalton Trans.* **2012**, *41*, 13556–13567; b) L. Sorace, C. Benelli, D. Gatteschi, *Chem. Soc. Rev.* **2011**, *40*, 3092–3104; c) R. Sessoli, A. K. Powell, *Coord. Chem. Rev.* **2009**, *253*, 2328–2341.

[3] a) D. Gatteschi, L. Sorace, *J. Solid State Chem.* **2001**, *159*, 253–261; b) W. Wernsdorfer, N. E. Chakov, G. Christou, *Phys. Rev. B* **2004**, *70*, 132413; c) N. Iwahara, L. F. Chibotaru, *Sci. Rep.* **2016**, *6*, 24743; d) T. Gupta, G. Rajaraman, *Chem. Commun.* **2016**, *52*, 8972–9008; e) P. Jacobson, T. Herden, M. Muenks, G. Laskin, O. Brovko, V. Stepanyuk, M. Ternes, K. Kern, *Nat. Commun.* **2015**, *6*, 8536; f) S. Gómez-Coca, A. Urtizberea, E. Cremades, P. J. Alonso, A. Camón, E. Ruiz, F. Luis, *Nat. Commun.* **2014**, *5*, 4300; g) M. E. Boulon, G. Cucinotta, J. Luzon, C. Degl'Innocenti, M. Perfetti, K. Bernot, G. Calvez, A. Caneschi, R. Sessoli, *Angew. Chem. Int. Ed.* **2013**, *52*, 350–354; *Angew. Chem.* **2013**, *125*, 368; h) M. Murugesu, *Nat. Chem.* **2012**, *4*, 347–348; i) L. Ungur, L. F. Chibotaru, *Phys. Chem. Chem. Phys.* **2011**, *13*, 20086–20090; j) J. D. Rinehart, J. R. Long, *Chem. Sci.* **2011**, *2*, 2078–2085; k) T. Kajiwara, M. Nakano, K. Takahashi, S. Takaishi, M. Yamashita, *Chem. Eur. J.* **2011**, *17*, 196–205; l) J. Cirera, E. Ruiz, S. Alvarez, F. Neese, J. Kortus, *Chem. Eur. J.* **2009**, *15*, 4078–4087.

[4] a) N. Ishikawa, M. Sugita, W. Wernsdorfer, *Angew. Chem. Int. Ed.* **2005**, *44*, 2931–2935; *Angew. Chem.* **2005**, *117*, 2991; b) D. Gatteschi, R. Sessoli, *Angew. Chem. Int. Ed.* **2003**, *42*, 268–297; *Angew. Chem.* **2003**, *115*, 278; c) W. Wernsdorfer, S. Bhaduri, C. Boskovic, G. Christou, D. N. Hendrickson, *Phys. Rev. B* **2002**, *65*, 180403–180404; d) E. K. Brechin, C. Boskovic, W. Wernsdorfer, J. Yoo, A. Yamaguchi, E. C. Sañudo, T. R. Concolino, A. L. Rheingold, H. Ishimoto, D. N. Hendrickson, G. Christou, *J. Am. Chem. Soc.* **2002**, *124*, 9710–9711; e) B. Barbara, L. Thomas, F. Lionti, I. Chiorescu, A. Sulpice, *J. Magn. Magn. Mater.* **1999**, *200*, 167–181.

[5] International Business Machines (IBM), *Vol. 2012*, **2012**.

[6] a) H. Hao, X. Zheng, T. Jia, Z. Zeng, *RSC Adv.* **2015**, *5*, 54667–54671; b) L. Rosado Piquer, E. C. Sanudo, *Dalton Trans.* **2015**, *44*, 8771–8780.

[7] M. Manoli, A. Collins, S. Parsons, A. Candini, M. Evangelisti, E. K. Brechin, *J. Am. Chem. Soc.* **2008**, *130*, 11129–11139.

[8] a) S. Sanvito, *Chem. Soc. Rev.* **2011**, *40*, 3336–3355; b) A. Soncini, L. F. Chibotaru, *Phys. Rev. B* **2010**, *81*, 132403; c) J. R. Friedman, M. P. Sarachik, *Annu. Rev. Condens. Matter Phys.* **2010**, *1*, 109–128; d) E. Coronado, A. J. Epsetin, *J. Mater. Chem.* **2009**, *19*, 1670–1671; e) N. Roch, S. Florens, V. Bouchiat, W. Wernsdorfer, F. Balestro, *Nature* **2008**, *453*, 633–U633; f) L. Bogani, W. Wernsdorfer, *Nat. Mater.* **2008**, *7*, 179–186; g) M. N. Leuenberger, D. Loss, *Phys. E* **2001**, *10*, 452–457; h) E. Coronado, M. Yamashita, *Dalton Trans.* **2016**, *45*, 16553–16555.

[9] a) Y.-S. Ding, N. F. Chilton, R. E. P. Winpenny, Y.-Z. Zheng, *Angew. Chem. Int. Ed.* **2016**, *55*, 16071–16074; *Angew. Chem.* **2016**, *128*, 16305; b) J. Liu, Y.-C. Chen, J.-H. Jia, J.-L. Liu, V. Vieru, L. Ungur, L. F. Chibotaru, Y. Lan, W. Wernsdorfer, S. Gao, X.-M. Chen, M.-L. Tong, *J. Am. Chem. Soc.* **2016**, *138*, 5441–5450; c) Y.-C. Chen, J.-L. Liu, L. Ungur, J. Liu, Q.-W. Li, L.-F. Wang, Z.-P. Ni, L. F. Chibotaru, X.-M. Chen, M.-L. Tong, *J. Am. Chem. Soc.* **2016**, *138*, 2829–2837; d) S. K. Gupta, T. Rajeshkumar, G. Rajaraman, R. Murugavel, *Chem. Commun.* **2016**, *52*, 7168–7171; e) S. K. Gupta, T. Rajeshkumar, G. Rajaraman, R. Murugavel, *Chem. Sci.* **2016**, *7*, 5181–5191; f) C. R. Ganivet, B. Ballesteros, G. de la Torre, J. M. Clemente-Juan, E. Coronado, T. Torres, *Chem. Eur. J.* **2013**, *19*, 1457–1465.

[10] a) N. F. Chilton, *Inorg. Chem.* **2015**, *54*, 2097–2099; b) N. F. Chilton, C. A. P. Goodwin, D. P. Mills, R. E. P. Winpenny, *Chem. Commun.* **2015**, *51*, 101–103; c) M. Gregson, N. F. Chilton, A.-M. Ariciu, F. Tuna, I. F. Crowe, W. Lewis, A. J. Blake, D. Collison, E. J. L. McInnes, R. E. P. Winpenny, S. T. Liddle, *Chem. Sci.* **2016**, *7*, 155–165; d) S. K. Langley, D. P. Wielechowski, B. Moubaraki, K. S. Murray, *Chem. Commun.* **2016**, *52*, 10976–10979; e) G. Cucinotta, M. Perfetti, J. Luzon, M. Etienne, P. E. Car, A. Caneschi, G. Calvez, K. Bernot, R. Sessoli, *Angew. Chem. Int. Ed.* **2012**, *51*, 1606–1610; *Angew. Chem.* **2012**, *124*, 1638.

[11] a) L. Ungur, J. J. Le Roy, I. Korobkov, M. Murugesu, L. F. Chibotaru, *Angew. Chem. Int. Ed.* **2014**, *53*, 4413–4417; *Angew. Chem.* **2014**, *126*, 4502; b) S. Zhang, H. Ke, L. Sun, X. Li, Q. Shi, G. Xie, Q. Wei, D. Yang, W. Wang, S. Chen, *Inorg. Chem.* **2016**, *55*, 3865–3871; c) W.-B. Sun, P.-F. Yan, S.-D. Jiang, B.-W. Wang, Y.-Q. Zhang, H.-F. Li, P. Chen, Z.-M. Wang, S. Gao, *Chem. Sci.* **2016**, *7*, 684–691; d) Y. Rechkemmer, J. E. Fischer, R. Marx, M. Dörfel, P. Neugebauer, S. Horvath, M. Gysler, T. Brock-Nannestad, W. Frey, M. F.

Reid, J. van Slageren, *J. Am. Chem. Soc.* **2015**, *137*, 13114–13120; e) S.-Y. Lin, C. Wang, L. Zhao, J. Wu, J. Tang, *Dalton Trans.* **2015**, *44*, 223–229; f) Q.-W. Li, J.-L. Liu, J.-H. Jia, Y.-C. Chen, J. Liu, L.-F. Wang, M.-L. Tong, *Chem. Commun.* **2015**, *51*, 10291–10294; g) A. K. Mondal, S. Goswami, S. Konar, *Dalton Trans.* **2015**, *44*, 5086–5094; h) Y.-L. Wang, B. Gu, Y. Ma, C. Xing, Q.-L. Wang, L.-C. Li, P. Cheng, D.-Z. Liao, *CrystEngComm* **2014**, *16*, 2283–2289; i) G. Rajaraman, S. K. Singh, T. Gupta, M. Shanmugam, *Chem. Commun.* **2014**, *50*, 15513–15516; j) K. S. Pedersen, L. Ungur, M. Sigrist, A. Sundt, M. Schau-Magnussen, V. Vieru, H. Mutka, S. Rols, H. Weihe, O. Waldmann, L. F. Chibotaru, J. Bendix, J. Dreiser, *Chem. Sci.* **2014**, *5*, 1650–1660; k) L. J. Batchelor, I. Cimatti, R. Guillot, F. Tuna, W. Wernsdorfer, L. Ungur, L. F. Chibotaru, V. E. Campbell, T. Mallah, *Dalton Trans.* **2014**, *43*, 12146–12149; l) S. Cardona-Serra, J. M. Clemente-Juan, E. Coronado, A. Gaita-Arino, A. Camon, M. Evangelisti, F. Luis, M. J. Martinez-Perez, J. Sese, *J. Am. Chem. Soc.* **2012**, *134*, 14982–14990; m) K. Bernot, J. Luzon, L. Bogani, M. Etienne, C. Sangregorio, M. Shanmugam, A. Caneschi, R. Sessoli, D. Gatteschi, *J. Am. Chem. Soc.* **2009**, *131*, 5573–5579; n) S. K. Langley, D. P. Wielechowski, V. Vieru, N. F. Chilton, B. Moubaraki, B. F. Abrahams, L. F. Chibotaru, K. S. Murray, *Angew. Chem. Int. Ed.* **2013**, *52*, 12014–12019; *Angew. Chem.* **2013**, *125*, 12236; o) K. S. Pedersen, M. Schau-Magnussen, J. Bendix, H. Weihe, A. V. Palii, S. I. Klokishner, S. Ostrovsky, O. S. Reu, H. Mutka, P. L. W. Tregenna-Piggott, *Chem. Eur. J.* **2010**, *16*, 13458–13464.

[12] a) M. Vonci, K. Mason, E. A. Suturina, A. T. Frawley, S. G. Worswick, I. Kuprov, D. Parker, E. J. L. McInnes, N. F. Chilton, *J. Am. Chem. Soc.* **2017**, *139*, 14166–14172; b) M. J. Giansiracusa, E. Moreno-Pineda, R. Hussain, R. Marx, M. Martínez Prada, P. Neugebauer, S. Al-Badran, D. Collison, F. Tuna, J. van Slageren, S. Carretta, T. Guidi, E. J. L. McInnes, R. E. P. Winpenny, N. F. Chilton, *J. Am. Chem. Soc.* **2018**, *140*, 2504–2513.

[13] a) J. Long, J. Rouquette, J.-M. Thibaud, R. A. S. Ferreira, L. D. Carlos, B. Donnadieu, V. Vieru, L. F. Chibotaru, L. Konczewicz, J. Haines, Y. Guari, J. Larionova, *Angew. Chem. Int. Ed.* **2015**, *54*, 2236–2240; *Angew. Chem.* **2015**, *127*, 2264; b) J. Zhu, C. Wang, F. Luan, T. Liu, P. Yan, G. Li, *Inorg. Chem.* **2014**, *53*, 8895–8901; c) G. Xiong, X. Y. Qin, P. F. Shi, Y. L. Hou, J. Z. Cui, B. Zhao, *Chem. Commun.* **2014**, *50*, 4255–4257; d) B. Na, X.-J. Zhang, W. Shi, Y.-Q. Zhang, B.-W. Wang, C. Gao, S. Gao, P. Cheng, *Chem. Eur. J.* **2014**, *20*, 15975–15980; e) G.-J. Chen, Y. Zhou, G.-X. Jin, Y.-B. Dong, *Dalton Trans.* **2014**, *43*, 16659–16665; f) Z.-G. Wang, J. Lu, C.-Y. Gao, C. Wang, J.-L. Tian, W. Gu, X. Liu, S.-P. Yan, *Inorg. Chem. Commun.* **2013**, *27*, 127–130; g) Y.-L. Wang, Y. Ma, X. Yang, J. Tang, P. Cheng, Q.-L. Wang, L.-C. Li, D.-Z. Liao, *Inorg. Chem.* **2013**, *52*, 7380–7386; h) A. Venugopal, F. Tuna, T. P. Spaniol, L. Ungur, L. F. Chibotaru, J. Okuda, R. A. Layfield, *Chem. Commun.* **2013**, *49*, 901–903; i) M. Ren, D. Pinkowicz, M. Yoon, K. Kim, L. M. Zheng, B. K. Breedlove, M. Yamashita, *Inorg. Chem.* **2013**, *52*, 8342–8348; j) D. Prodius, F. Macaev, Y. Lan, G. Novitchi, S. Pogrebnoi, E. Stingaci, V. Mereacre, C. E. Anson, A. K. Powell, *Chem. Commun.* **2013**, *49*, 9215–9217; k) G. J. Chen, Y. N. Guo, J. L. Tian, J. Tang, W. Gu, X. Liu, S. P. Yan, P. Cheng, D. Z. Liao, *Chem. Eur. J.* **2012**, *18*, 2484–2487; l) D.-P. Li, X.-P. Zhang, T.-W. Wang, B.-B. Ma, C.-H. Li, Y.-Z. Li, X.-Z. You, *Chem. Commun.* **2011**, *47*, 6867–6869.

[14] a) N. Ishikawa, M. Sugita, N. Tanaka, T. Ishikawa, S.-y. Koshihara, Y. Kaizu, *Inorg. Chem.* **2004**, *43*, 5498–5500; b) R. J. Blagg, L. Ungur, F. Tuna, J. Speak, P. Comar, D. Collison, W. Wernsdorfer, E. J. L. McInnes, L. F. Chibotaru, R. E. P. Winpenny, *Nat. Chem.* **2013**, *5*, 673–678; c) J.-L. Liu, J.-Y. Wu, Y.-C. Chen, V. Mereacre, A. K. Powell, L. Ungur, L. F. Chibotaru, X.-M. Chen, M.-L. Tong, *Angew. Chem. Int. Ed.* **2014**, *53*, 12966–12970; *Angew. Chem.* **2014**, *126*, 13180; d) Y.-N. Guo, L. Ungur, G. E. Granroth, A. K. Powell, C. Wu, S. E. Nagler, J. Tang, L. F. Chibotaru, D. Cui, *Sci. Rep.* **2014**, *4*, 5471.

[15] a) J. Tang, P. Zhang in *Lanthanide Single Molecule Magnets*, Springer, Berlin, **2015**; b) S. Gao (Ed.), *Molecular Nanomagnets and Related Phenomena*, Springer, Berlin, **2015**.

[16] A. Burrows, *Chemistry 3: Introducing Inorganic, Organic and Physical Chemistry*, Oxford University Press, Oxford, **2009**.

[17] A. K. Zvezdin, V. M. Matveev, A. A. Mukhin, A. I. Popov, *Rare-Earth Ions in Ordered Magnetic Crystals*, Nauka, Moscow, **1985**, pp. 296.

[18] a) H. U. Gudel, U. Hauser, A. Furrer, *Inorg. Chem.* **1979**, *18*, 2730–2737; b) G. Amoretti, R. Caciuffo, S. Carretta, T. Guidi, N. Magnani, P. Santini, *Inorg. Chim. Acta* **2008**, *361*, 3771–3776.

[19] a) A. Bencini, D.Gatteschi, *Electron Paramagnetic Resonance of Exchange Coupled Systems*, Springer-Verlag, Berlin, **1990**; b) A. L. Barra, D. Gatteschi, R. Sessoli, G. L. Abbati, A. Cornia, A. C. Fabretti, M. G. Uytterhoeven, *Angew. Chem. Int. Ed. Engl.* **1997**, *36*, 2329–2331; *Angew. Chem.* **1997**, *109*, 2423.

[20] a) M. Perfetti, *Coord. Chem. Rev.* **2017**, *348*, 171–186; b) M. Perfetti, E. Lucaccini, L. Sorace, J. P. Costes, R. Sessoli, *Inorg. Chem.* **2015**, *54*, 3090–3092; c) A. Cornia, D. Gatteschi, R. Sessoli, *Coord. Chem. Rev.* **2001**, *219–221*, 573–604.

[21] a) A. T. Coomber, R. H. Friend, A. Charlton, A. E. Underhill, M. Kurmoo, P. Day, *Mol. Cryst. Liq. Cryst.* **1995**, *273*, 41–45; b) L. D. Tung, J. Schefer, M. R. Lees, G. Balakrishnan, D. M. Paul, *J. Sci.: Adv. Mater. Dev.* **2016**, *1*, 174–178; c) M. Blankenhorn, E. Heintze, M. Slota, J. van Slageren, B. A. Moores, C. L. Degen, L. Bogani, M. Dressel, *Rev. Sci. Instrum.* **2017**, *88*, 094707.

[22] a) L. F. Chibotaru, L. Ungur, A. Soncini, *Angew. Chem. Int. Ed.* **2008**, *47*, 4126–4129; *Angew. Chem.* **2008**, *120*, 4194; b) L. F. Chibotaru, L. Ungur, C. Aronica, H. Elmoll, G. Pilet, D. Luneau, *J. Am. Chem. Soc.* **2008**, *130*, 12445–12455; c) J. P. Costes, S. Titos-Padilla, I. Oyarzabal, T. Gupta, C. Duhayon, G. Rajaraman, E. Colacio, *Inorg. Chem.* **2016**, *55*, 4428–4440; d) S. K. Singh, T. Gupta, L. Ungur, G. Rajaraman, *Chem. Eur. J.* **2015**, *21*, 13812–13819; e) C. Das, S. Vaidya, T. Gupta, J. M. Frost, M. Righi, E. K. Brechin, M. Affronte, G. Rajaraman, M. Shanmugam, *Chem. Eur. J.* **2015**, *21*, 15639–15650; f) J. P. Costes, S. Titos-Padilla, I. Oyarzabal, T. Gupta, C. Duhayon, G. Rajaraman, E. Colacio, *Chem. Eur. J.* **2015**, *21*, 15785–15796; g) S. K. Singh, T. Gupta, G. Rajaraman, *Inorg. Chem.* **2014**, *53*, 10835–10845; h) T. Gupta, G. Rajaraman, *J. Chem. Sci.* **2014**, *126*, 1569–1579; i) T. Gupta, G. Velmurugan, T. Rajeshkumar, G. Rajaraman, *J. Chem. Sci.* **2016**, *128*, 1615–1630; j) L. Ungur, L. F. Chibotaru, *Inorg. Chem.* **2016**, *55*, 10043–10056; k) T. Pugh, V. Vieru, L. F. Chibotaru, R. A. Layfield, *Chem. Sci.* **2016**, *7*, 2128–2137; l) M. Gysler, F. El Hallak, L. Ungur, R. Marx, M. Hakl, P. Neugebauer, Y. Rechkemmer, Y. Lan, I. Sheikin, M. Orlita, C. E. Anson, A. K. Powell, R. Sessoli, L. F. Chibotaru, J. van Slageren, *Chem. Sci.* **2016**, *7*, 4347–4354; m) X. Zhang, V. Vieru, X. Feng, J.-L. Liu, Z. Zhang, B. Na, W. Shi, B.-W. Wang, A. K. Powell, L. F. Chibotaru, S. Gao, P. Cheng, J. R. Long, *Angew. Chem. Int. Ed.* **2015**, *54*, 9861–9865; *Angew. Chem.* **2015**, *127*, 9999; n) S. Xue, Y.-N. Guo, L. Ungur, J. Tang, L. F. Chibotaru, *Chem. Eur. J.* **2015**, *21*, 14099–14106; o) L. Ungur, L. F. Chibotaru in *Lanthanides and Actinides in Molecular Magnetism* (Eds: R. A. Layfield, M. Murugesu), Wiley-VCH Verlag GmbH & Co. KGaA, Weinheim, **2015**, pp. 153–184; p) T. Pugh, F. Tuna, L. Ungur, D. Collison, E. J. L. McInnes, L. F. Chibotaru, R. A. Layfield, *Nat. Commun.* **2015**, *6*, 7492; q) J.-L. Liu, J.-Y. Wu, G.-Z. Huang, Y.-C. Chen, J.-H. Jia, L. Ungur, L. F. Chibotaru, X.-M. Chen, M.-L. Tong, *Sci. Rep.* **2015**, *5*, 16621; r) S. K. Langley, D. P. Wielechowski, V. Vieru, N. F. Chilton, B. Moubaraki, L. F. Chibotaru, K. S. Murray, *Chem. Commun.* **2015**, *51*, 2044–2047; s) X.-C. Huang, V. Vieru, L. F. Chibotaru, W. Wernsdorfer, S.-D. Jiang, X.-Y. Wang, *Chem. Commun.* **2015**, *51*, 10373–10376; t) L. Chibotaru in *Molecular Nanomagnets and Related Phenomena, Vol. 164* (Ed.: S. Gao), Springer, Berlin, **2015**, pp. 185–229; u) S. Xue, L. Ungur, Y.-N. Guo, J. Tang, L. F. Chibotaru, *Inorg. Chem.* **2014**, *53*, 12658–12663.

[23] B. Swerts, L. F. Chibotaru, R. Lindh, L. Seijo, Z. Barandiaran, S. Clima, K. Pierloot, M. F. A. Hendrickx, *J. Chem. Theory Comput.* **2008**, *4*, 586–594.

[24] P. A. Malmqvist, B. O. Roos, B. Schimmelpfennig, *Chem. Phys. Lett.* **2002**, *357*, 230–240.

[25] a) L. F. Chibotaru, L. Ungur, University of Leuven, Belgium, **2006**; b) L. Ungur, L. F. Chibotaru in http://www.molcas.org/documentation/manual/node105.html; c) L. F. Chibotaru, L. Ungur, *J. Chem. Phys.* **2012**, *137*, 064112–064122; d) L. Chibotaru, A. Ceulemans, H. Bolvin, *Phys. Rev. Lett.* **2008**, *101*, 033003–033001.

[26] a) F. Aquilante, J. Autschbach, R. K. Carlson, L. F. Chibotaru, M. G. Delcey, L. De Vico, I. Fdez Galván, N. Ferré, L. M. Frutos, L. Gagliardi, M. Garavelli, A. Giussani, C. E. Hoyer, G. Li Manni, H. Lischka, D. Ma, P. Å. Malmqvist, T. Müller, A. Nenov, M. Olivucci, T. B. Pedersen, D. Peng, F. Plasser, B. Pritchard, M. Reiher, I. Rivalta, I. Schapiro, J. Segarra-Martí, M. Stenrup, D. G. Truhlar, L. Ungur, A. Valentini, S. Vancoillie, V. Veryazov, V. P. Vysotskiy, O. Weingart, F. Zapata, R. Lindh, *J. Comput. Chem.* **2016**, *37*, 506–541; b) F. Aquilante, L. De Vico, N. Ferre, G. Ghigo, P. A. Malmqvist, P. Neogrady, T. B. Pedersen, M. Pitonak, M. Reiher, B. O. Roos, L. Serrano-Andres, M. Urban, V. Veryazov, R. Lindh, *J. Comput. Chem.* **2010**, *31*, 224–247; c) J. A. Duncan, *J. Am. Chem. Soc.* **2009**, *131*, 2416–2416; d) V. Veryazov, P. O. Widmark, L. Serrano-Andres, R. Lindh, B. O. Roos, *Int. J. Quantum Chem.* **2004**, *100*, 626–635; e) G. Karlstrom, R. Lindh, P. A. Malmqvist,

B. O. Roos, U. Ryde, V. Veryazov, P. O. Widmark, M. Cossi, B. Schimmelpfennig, P. Neogrady, L. Seijo, *Comput. Mater. Sci.* **2003**, *28*, 222–239.
[27] U. J. Williams, B. D. Mahoney, P. T. DeGregorio, P. J. Carroll, E. Nakamaru-Ogiso, J. M. Kikkawa, E. J. Schelter, *Chem. Commun.* **2012**, *48*, 5593–5595.
[28] T. Gupta, T. Rajeshkumar, G. Rajaraman, *Phys. Chem. Chem. Phys.* **2014**, *16*, 14568–14577.
[29] B. O. Roos, R. Lindh, P. A. Malmqvist, V. Veryazov, P. O. Widmark, A. C. Borin, *J. Phys. Chem. A* **2008**, *112*, 11431–11435.
[30] M. J. Frisch, G. W. Trucks, H. B. Schlegel, G. E. Scuseria, M. A. Robb, J. R. Cheeseman, G. Scalmani, V. Barone, B. Mennucci, G. A. Petersson, H. Nakatsuji, M. Caricato, X. Li, H. P. Hratchian, A. F. Izmaylov, J. Bloino, G. Zheng, J. L. Sonnenberg, M. Hada, M. Ehara, K. Toyota, R. Fukuda, J. Hasegawa, M. Ishida, T. Nakajima, Y. Honda, O. Kitao, H. Nakai, T. Vreven, J. A. Montgomery Jr., J. E. Peralta, F. Ogliaro, M. Bearpark, J. J. Heyd, E. Brothers, K. N. Kudin, V. N. Staroverov, R. Kobayashi, J. Normand, K. Raghavachari, A. Rendell, J. C. Burant, S. S. Iyengar, J. Tomasi, M. Cossi, N. Rega, J. M. Millam, M. Klene, J. E. Knox, J. B. Cross, V. Bakken, C. Adamo, J. Jaramillo, R. Gomperts, R. E. Stratmann, O. Yazyev, A. J. Austin, R. Cammi, C. Pomelli, J. W. Ochterski, R. L. Martin, K. Morokuma, V. G. Zakrzewski, G. A. Voth, P. Salvador, J. J. Dannenberg, S. Dapprich, A. D. Daniels, Ö. Farkas, J. B. Foresman, J. V. Ortiz, J. Cioslowski, D. J. Fox, *Gaussian 09, Revision A.02* Gaussian, Inc., Wallingford CT, **2009**.
[31] a) A. D. Becke, *J. Chem. Phys.* **1993**, *98*, 5648–5652; b) A. D. Becke, *Phys. Rev. A* **1988**, *38*, 3098–3100; c) C. T. Lee, W. T. Yang, R. G. Parr, *Phys. Rev. B* **1988**, *37*, 785–789; d) P. J. Stephens, F. J. Devlin, C. F. Chabalowski, M. J. Frisch, *J. Phys. Chem.* **1994**, *98*, 11623–11627.
[32] T. R. Cundari, W. J. Stevens, *J. Chem. Phys.* **1993**, *98*, 5555–5565.
[33] A. Schafer, C. Huber, R. Ahlrichs, *J. Chem. Phys.* **1994**, *100*, 5829–5835.
[34] E. Moreno Pineda, N. F. Chilton, R. Marx, M. Dörfel, D. O. Sells, P. Neugebauer, S.-D. Jiang, D. Collison, J. van Slageren, E. J. L. McInnes, R. E. P. Winpenny, *Nat. Commun.* **2014**, *5*, 5243.
[35] a) J. Ruiz, A. J. Mota, A. Rodriguez-Dieguez, S. Titos, J. M. Herrera, E. Ruiz, E. Cremades, J. P. Costes, E. Colacio, *Chem. Commun.* **2012**, *48*, 7916–7918; b) S. Titos-Padilla, J. Ruiz, J. M. Herrera, E. K. Brechin, W. Wersndorfer, F. Lloret, E. Colacio, *Inorg. Chem.* **2013**, *52*, 9620–9626; c) M. M. Hänninen, A. J. Mota, D. Aravena, E. Ruiz, R. Sillanpää, A. Camón, M. Evangelisti, E. Colacio, *Chem. Eur. J.* **2014**, *20*, 8410–8420; d) I. Oyarzabal, J. Ruiz, E. Ruiz, D. Aravena, J. M. Seco, E. Colacio, *Chem. Commun.* **2015**, *51*, 12353–12356; e) S. Das, K. S. Bejoymohandas, A. Dey, S. Biswas, M. L. P. Reddy, R. Morales, E. Ruiz, S. Titos-Padilla, E. Colacio, V. Chandrasekhar, *Chem. Eur. J.* **2015**, *21*, 6449–6464; f) J. Ruiz, G. Lorusso, M. Evangelisti, E. K. Brechin, S. J. A. Pope, E. Colacio, *Inorg. Chem.* **2014**, *53*, 3586–3594; g) I. Oyarzabal, J. Ruiz, J. M. Seco, M. Evangelisti, A. Camón, E. Ruiz, D. Aravena, E. Colacio, *Chem. Eur. J.* **2014**, *20*, 14262–14269; h) I. F. Díaz-Ortega, J. M. Herrera, D. Aravena, E. Ruiz, T. Gupta, G. Rajaraman, H. Nojiri, E. Colacio, *Inorg. Chem.* **2018**, *57*, 6362–6375; i) E. Lucaccini, L. Sorace, M. Perfetti, J.-P. Costes, R. Sessoli, *Chem. Commun.* **2014**, *50*, 1648–1651.
[36] D. Aravena, E. Ruiz, *Inorg. Chem.* **2013**, *52*, 13770–13778.
[37] a) S.-D. Jiang, S.-X. Qin, *Inorg. Chem. Front.* **2015**, *2*, 613–619; b) N. F. Chilton, S. K. Langley, B. Moubaraki, A. Soncini, S. R. Batten, K. S. Murray, *Chem. Sci.* **2013**, *4*, 1719–1730.
[38] R. Marx, F. Moro, M. Dorfel, L. Ungur, M. Waters, S. D. Jiang, M. Orlita, J. Taylor, W. Frey, L. F. Chibotaru, J. van Slageren, *Chem. Sci.* **2014**, *5*, 3287–3293.
[39] J. J. Le Roy, M. Jeletic, S. I. Gorelsky, I. Korobkov, L. Ungur, L. F. Chibotaru, M. Murugesu, *J. Am. Chem. Soc.* **2013**, *135*, 3502–3510.
[40] a) M. A. AlDamen, S. Cardona-Serra, J. M. Clemente-Juan, E. Coronado, A. Gaita-Arino, C. Marti-Gastaldo, F. Luis, O. Montero, *Inorg. Chem.* **2009**, *48*, 3467–3479; b) M. A. AlDamen, J. M. Clemente-Juan, E. Coronado, C. Marti-Gastaldo, A. Gaita-Arino, *J. Am. Chem. Soc.* **2008**, *130*, 8874–8875.
[41] O. Khalfaoui, A. Beghidja, J. Long, C. Beghidja, Y. Guari, J. Larionova, *Inorganics* **2018**, *6*, 35.
[42] C.-M. Liu, D.-Q. Zhang, X. Hao, D.-B. Zhu, *Sci. China Ser. B* **2017**, *60*, 358–365.
[43] G.-J. Chen, C.-Y. Gao, J.-L. Tian, J. Tang, W. Gu, X. Liu, S.-P. Yan, D.-Z. Liao, P. Cheng, *Dalton Trans.* **2011**, *40*, 5579–5583.
[44] a) C. A. P. Goodwin, F. Ortu, D. Reta, N. F. Chilton, D. P. Mills, *Nature* **2017**, *548*, 439–442; b) A. Lunghi, F. Totti, S. Sanvito, R. Sessoli, *Chem. Sci.* **2017**, *8*, 6051–6059.
[45] Y. Kishi, F. Pointillart, B. Lefeuvre, F. Riobe, B. Le Guennic, S. Golhen, O. Cador, O. Maury, H. Fujiwara, L. Ouahab, *Chem. Commun.* **2017**, *53*, 3575–3578.
[46] N. Ishikawa, M. Sugita, T. Ishikawa, S. Koshihara, Y. Kaizu, *J. Am. Chem. Soc.* **2003**, *125*, 8694–8695.

Received: March 16, 2018